Supplementary Information

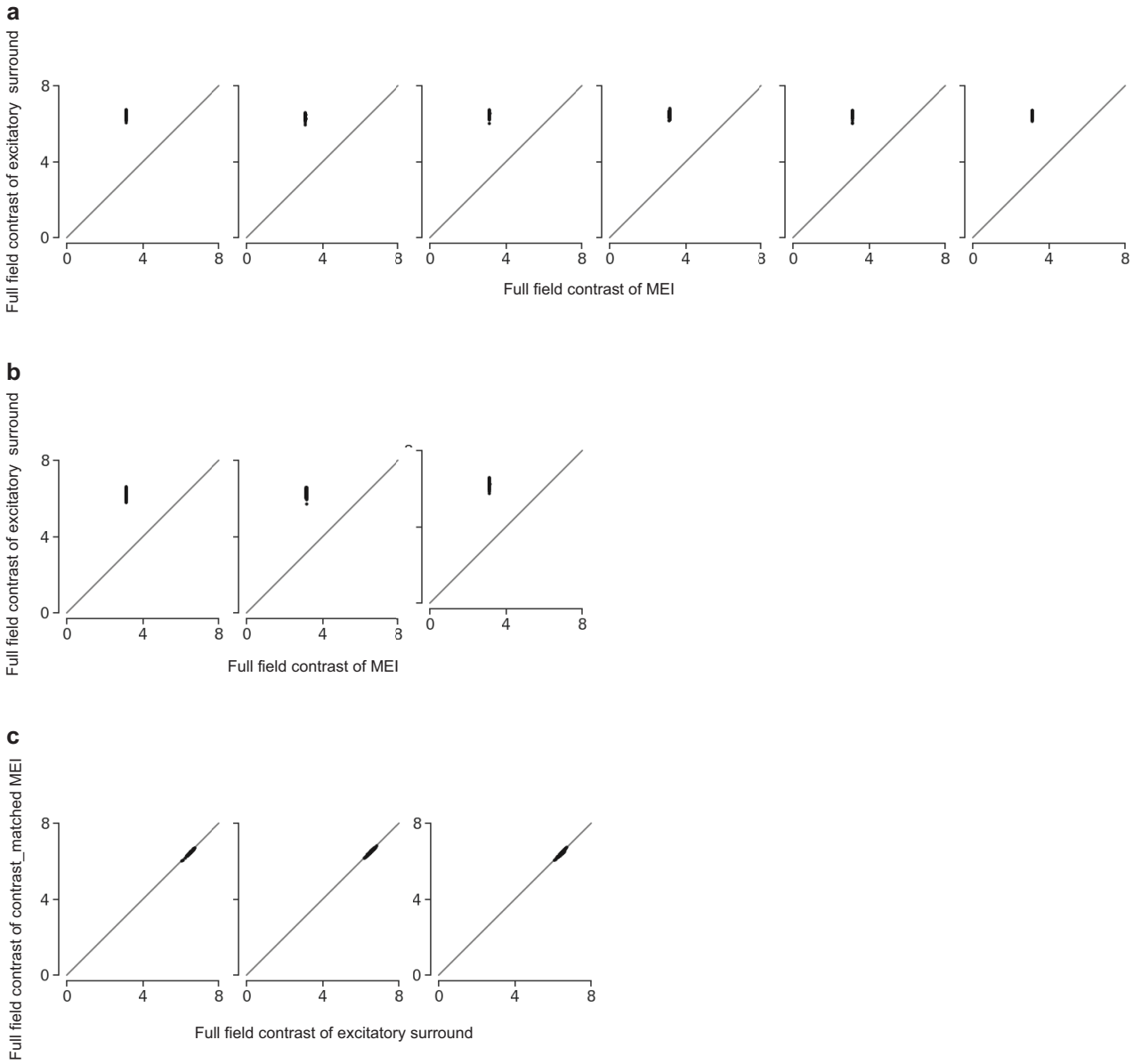

Supplemental Fig. 1. Comparison of stimulus contrast of MEIs and excitatory and inhibitory surround. a, Full-field RMS contrast comparison between the MEI (x-axis) and the excitatory surround images (y-axis) (n=6 animals, 960 cells total). **b,** Full-field RMS contrast comparison between the MEI (x-axis) and the inhibitory surround images (y-axis) (n=3 animals, 510 cells total). **c,** Full-field RMS contrast comparison between the excitatory surround image (x-axis) and the contrast-matched MEI (y-axis) (n=3 animals, 560 cells total).

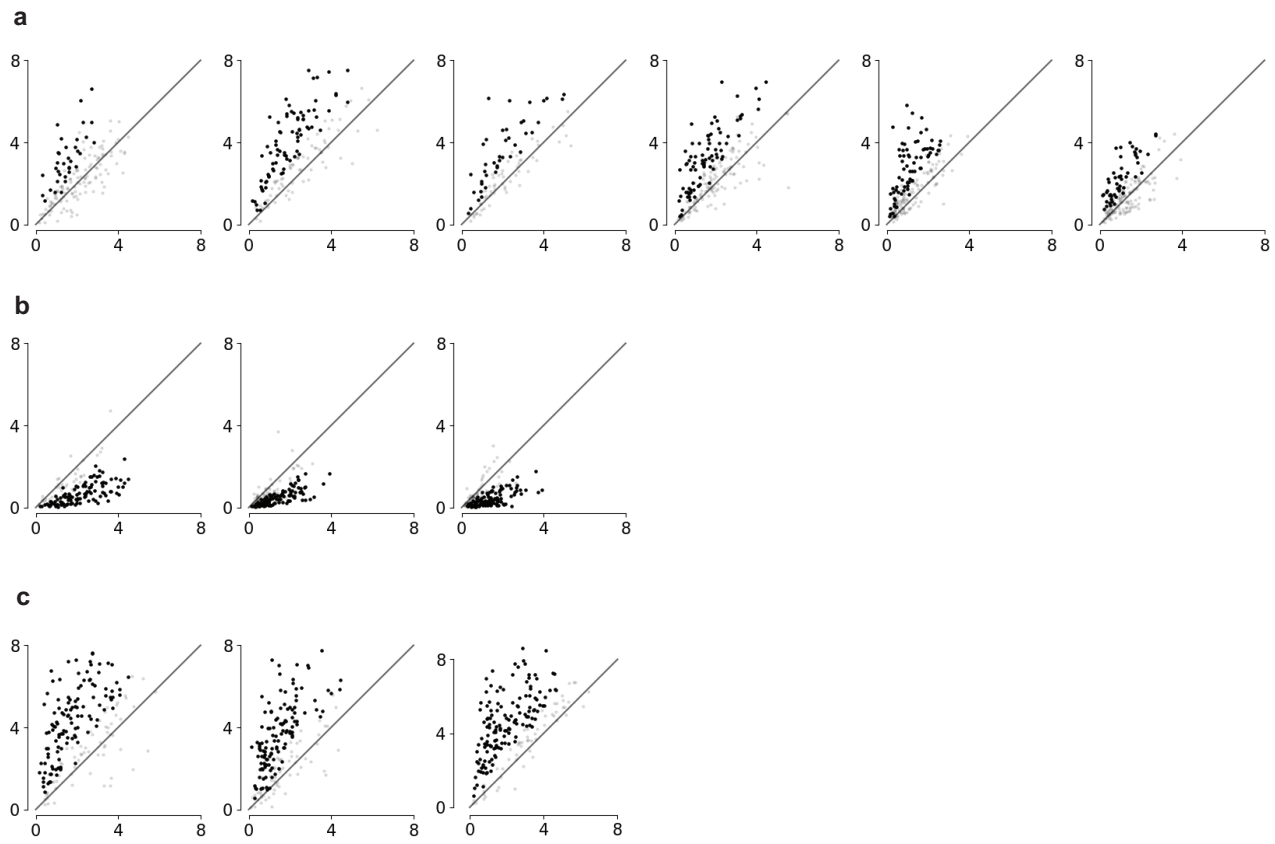

Supplemental Fig. 2. Neuronal responses to MEIs and surround imaged recorded during inception loop experiments. a, Comparing observed responses to the MEI (x-axis) and the excitatory surround (y-axis) per experiment (n=6 mice, 960 cells total). Dark dots indicate neurons where the response to the surround images is significantly higher than to the MEI (Wilcoxon rank-sum test, p-value<0.05). Across the population, the modulation was significant for all animals (p-value<0.05, Wilcoxon signed rank test). **b,** Comparing observed responses to the MEI (x-axis) and the inhibitory surround (y-axis) per experiment (n=3 mice, 510 cells total). Dark dots indicate neurons where the response to the surround images is significantly lower than to the MEI (Wilcoxon rank-sum test, p-value<0.05). Across the population, the modulation was significant for all animals (p-value<0.05, Wilcoxon signed rank test). **c,** Comparing observed responses to the excitatory surround (x-axis) and the contrast-matched MEI (y-axis) per experiment (n=3 mice, 560 cells total). Dark dots indicate neurons where the response to the contrast-matched MEIs is significantly higher than to the MEI (Wilcoxon rank-sum test, p-value<0.05). Across the population, the modulation was significant for all animals (p-value<0.05, Wilcoxon signed rank test).

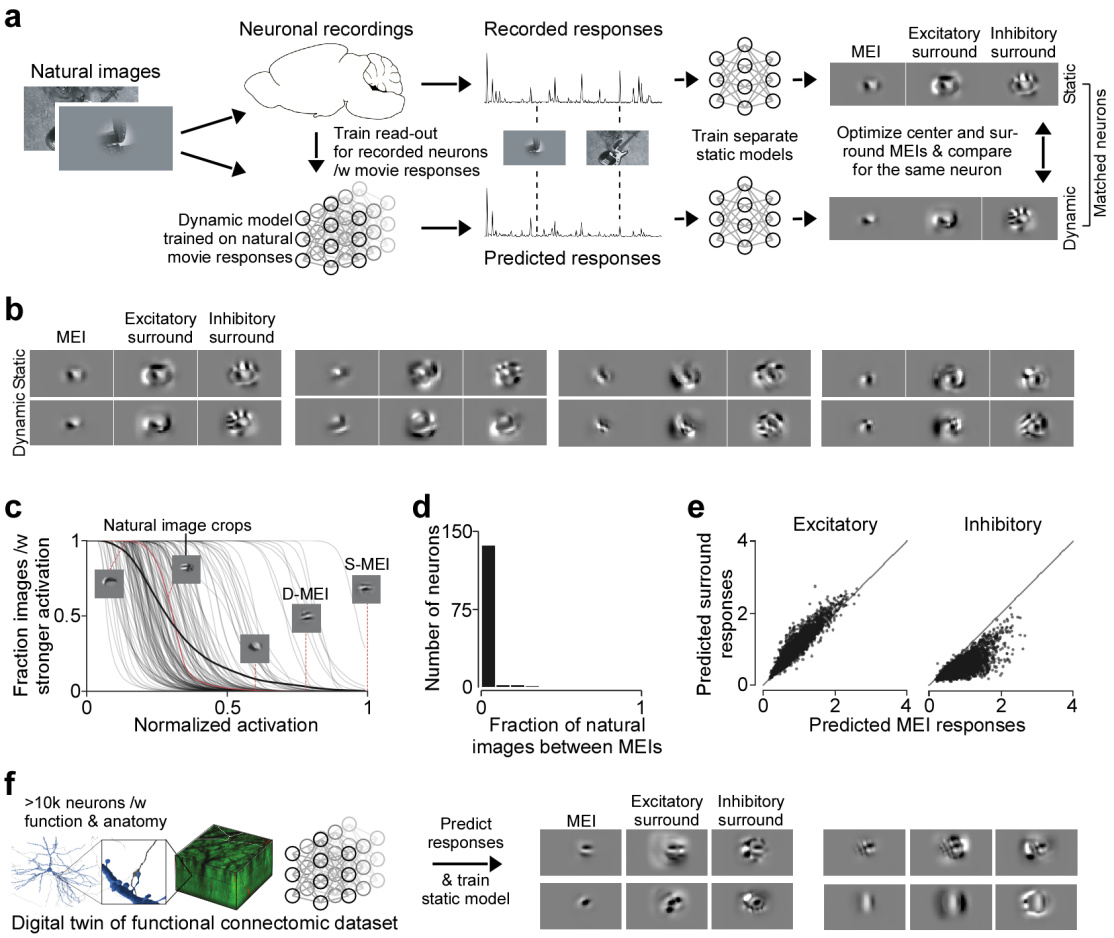

Supplemental Fig. 3. Contextual modulation is reproduced in digital twin of large-scale functional connectomics dataset. a, Circuit-level mechanistic explanations of neuronal function require the combination of functional recordings and anatomical analyses. This panel shows a schematic illustrating how we reproduced our findings regarding contextual modulation in a functional connectomic dataset, which includes responses of >75k neurons to full-field natural movies and the reconstructed sub-cellular connectivity of the same cells from electron microscopy data ("MICrONS" dataset (MICrONS Consortium et al., 2021)). Importantly, a dynamic model of this mouse visual cortex—digital twin—exhibits not only a high predictive performance for natural movies, but also accurate out-of-domain performance on other stimulus classes such as drifting Gabor filters, directional pink noise, and random dot kinematograms, allowing to present new stimuli to this digital twin model in order to relate specific functional properties to the neurons' connectivity and anatomical properties. To this end, we recorded the visual activity of the same neuronal population to static natural images as well as to the identical natural movies that were used in the MICrONS dataset. Based on the responses to static natural images we trained a static model as described above, and from the responses to natural movies we trained a dynamic model using a recurrent neural network architecture described in REF. We then presented the same static natural image set that we showed to the mice also to their dynamic model counterparts and trained a second static model using these predicted *in silico* responses. This enabled us to compare the MEIs and surround images for the same neurons generated from two different static models: one trained directly on responses from real neurons, and another trained on synthetic responses to static images from dynamic models (D-MEI and D-surround). **b,** Static and dynamic MEIs and surround images of four example neurons, matched across recordings using their anatomical position in a structural stack. Importantly, the MEIs and surround images optimized from these two models were perceptually very similar. **c,** To quantify this similarity, we presented both versions of MEIs and surround images to an independent static model trained on the same natural images and responses but initialized with a different random seed, thereby avoiding model-specific biases. The panel shows neuronal activation to natural image crops, normalized with respect to MEI activation. Gray lines show the fraction out of 5,000 images that elicit a given activation or higher for n=x example model neurons (mean in black). For a representative cell (red), we show MEI, D-MEI and image crops with different activations. **d,** Fraction of natural images that activate the neurons stronger than the D-MEIs. On the population level, the fraction of natural image crops with activations higher than the D-MEI was very small, demonstrating that D-MEIs strongly activate their corresponding neurons. **e,** D-MEI responses plotted versus responses to excitatory and inhibitory D-surround images predicted by an independent static model. This shows that the excitatory and inhibitory D-surround stimuli modulated V1 responses in the direction as predicted by the model. **e,** Finally, we used the above pipeline to optimize MEIs and surround images from example neurons of the MICrONS dataset itself. Schematic shows the MICrONS dataset (left) and MEIs with surround images of four example neurons of the MICrONS dataset are shown on the right. This allows future circuit dissections towards understanding the mechanism underlying center-surround interaction in mouse visual cortex.

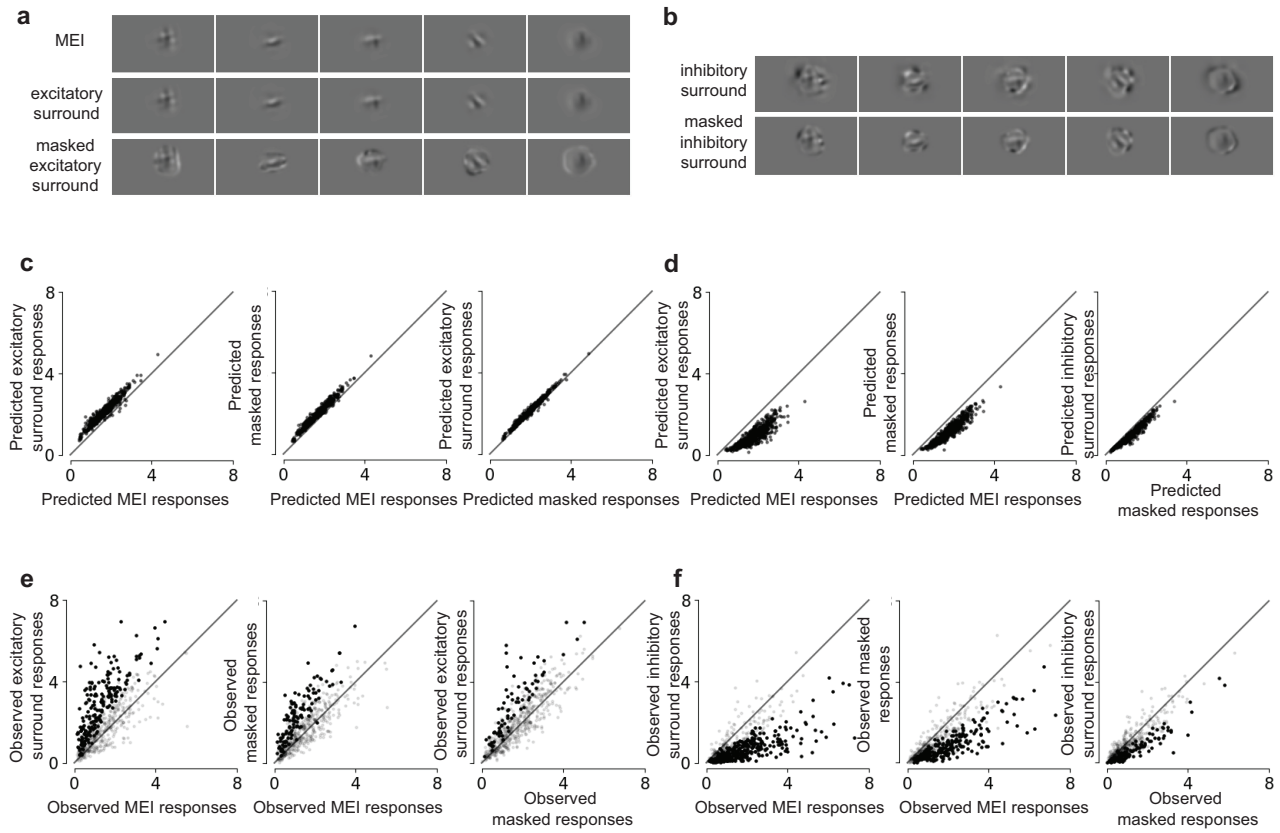

Supplemental Fig. 4. Images restricted to the far surround still result in surround modulation. a, Examples of the MEI, the excitatory surround and cropped excitatory surround. **b,** Examples of the MEI, the inhibitory surround and cropped inhibitory surround. **c,** Comparing predicted response to the MEI, the excitatory surround and the cropped surround image (n=3, 560 cells). **d,** Comparing predicted response to the MEI, the inhibitory surround and the cropped surround image (n=3, 560 cells). **e,** Comparing observed response to the MEI, the excitatory surround and the cropped surround image (n=3, 560 cells). Black dots indicate neurons with significantly higher response under the condition on the y-axis (one-sided Wilcoxon rank-sum test, p<0.05, 33.6%, 20.2% and 13.4% significant cells for each pair). Modulation is significant on population level for each pair (p-value=1.83×10^{-45}, 9.98×10^{-45}, 6.89×10^{-19}, Wilcoxon signed rank test). **f,** Comparing observed response to the MEI, the inhibitory surround and the cropped surround image (n=3, 560 cells). Black dots indicate neurons with significantly higher response under the condition on the y-axis (one-sided Wilcoxon rank-sum test, p<0.05, 55.9%, 40.3% and 19.6% significant cells for each pair). Modulation is significant on population level for each pair (p-value=8.05×10^{-73}, 9.03×10^{-66}, 2.42×10^{-24}, Wilcoxon signed rank test).

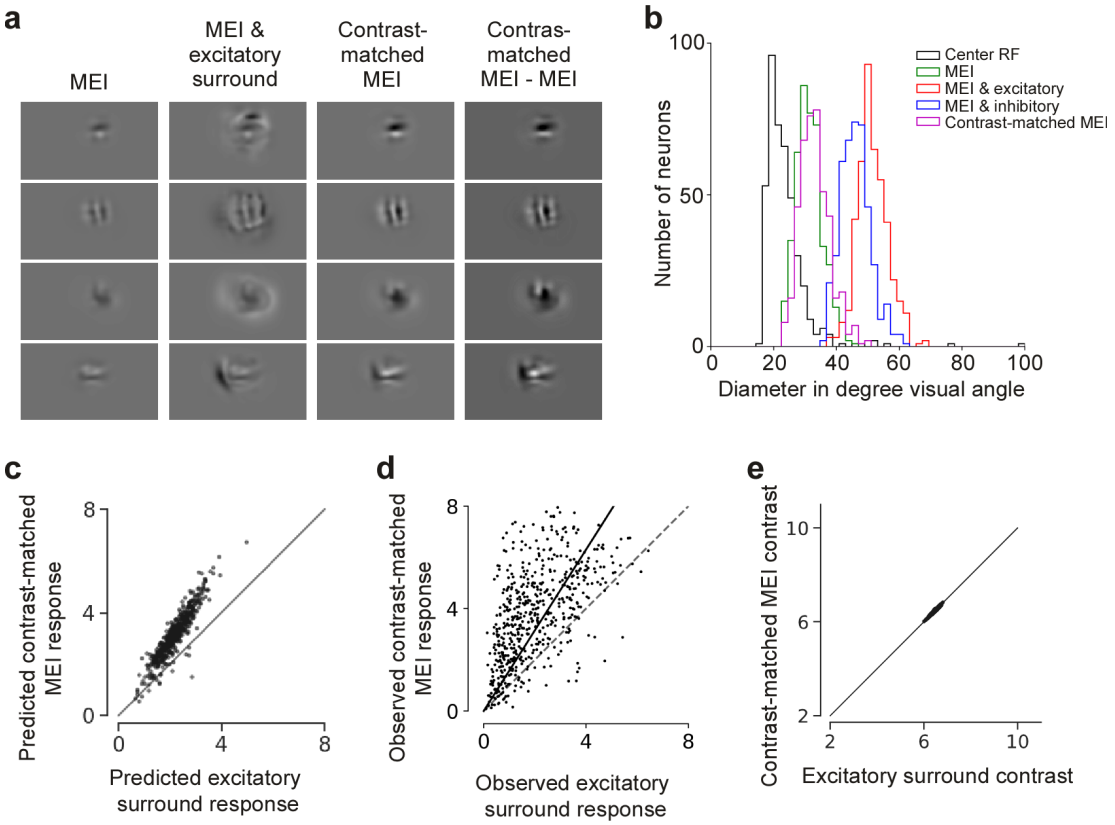

Supplemental Fig. 5. Contrast-matched MEIs result in higher activation than MEIs with excitatory surround. **a,** Panel shows MEI, excitatory surround with MEI, the contrast-matched MEI, and the difference between the original MEI and the contrast-matched MEI for 4 example neurons. Note that the contrast-matched MEI is a scaled-up version of the original MEI with same features. **b,** Diameters of RFs estimated using sparse noise, the MEIs, the MEIs with excitatory and inhibitory surround, and the contrast-matched MEI. Same data shown in Fig. 2e except for the contrast-matched MEI. The mean of the contrast-matched MEI (magenta distribution) size across all neurons (n=4, 434 cells) is 33.2 degrees $\pm$ 0.23 (mean $\pm$ s.e.m.). The size of the contrast-matched MEI is slightly larger than the original MEI (31.3 degrees $\pm$ 0.20). **c,** Model predicted responses to the MEI and excitatory surround (x-axis) and contrast-matched MEI (y-axis). Responses are depicted in arbitrary units, corresponding to the output of the model. **d,** Observed responses to the the MEI and excitatory surround (x-axis) and contrast-matched MEI (y-axis). For each neuron, responses are normalized by the standard deviation of responses to all images. Across the population, the neuronal responses to the contrast-matched MEI was significantly higher (p-value=7.35×10^{-80}, Wilcoxon signed rank test, slope of linear regression line=1.58). Across stimulus repetitions, 58.9% of the neurons responded stronger to the contrast-matched MEI (n=3 animals, 560 cells, two-sided t-test, p-value<0.05). Solid line indicates the regression line across the population, and dotted gray line indicates the diagonal. **e,** Contrast comparison between the MEI and excitatory surround (x-axis) and the contrast-matched MEI. By definition, the full-field contrast of each pair of images are matched.

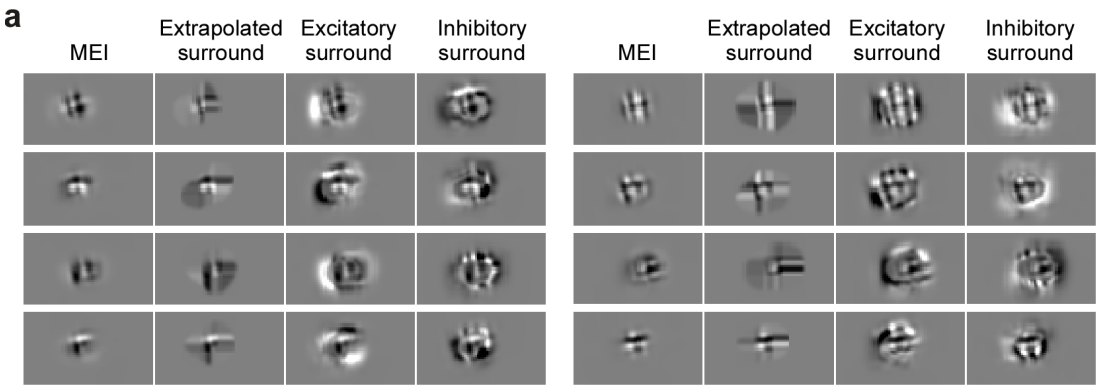

Supplemental Fig. 6. Surround images extrapolated from the spatial pattern of the MEI. a, MEIs, surround images extrapolated from the spatial pattern of the MEI and optimized excitatory and inhibitory surround images of example neurons.